Journal of the Physical Society of Japan
Vol. 69, No. 6, June, 2000, pp. 1865-1871

Canted Antiferromagnetic Order and Large Magnetoresistance Effect in $La_{1-X}Ca_XMnO_3$, $Pr_{1-X}Ca_XMnO_3$ and other $RE_{1-X}AE_XMnO_3$ Manganese Oxides ($X \sim 0.9$)

Hiroyuki FUJISHIRO, Manabu IKEBE, Shuichi OHSHIDEN and Koshichi NOTO

Faculty of Engineering, Iwate University, Morioka 020-8551

(Received January 17, 2000)

The magnetization M(T) and the electrical resistivity ρ(T) of lightly electron-doped $La_{1-X}Ca_XMnO_3$, $Pr_{1-X}Ca_XMnO_3$ and other $RE_{1-X}AE_XMnO_3$ (RE; rare-earth, AE; alkaline-earth) have been measured and the canted antiferromagnetic (CAF) phase which competes with the charge ordered (CO) phase has been extensively studied. The CAF phase was found to be more strongly stabilized for the smaller A-site ion radius of the perovskite structure. By systematically changing the concentration and the average A-site ion radius, a detailed phase diagram in the electron-doped region was established. The main origin of the CAF phase was suggested to be the antisymmetric exchange interaction associated with the G-type antiferromagnetic structure of these systems.

KEYWORDS: $RE_{1-X}Ca_XMnO_3$, $La_{1-X}(Ca_{1-y}Sr_y)_XMnO_3$, electron doping, canted antiferromagnetic order, charge order, magnetoresistance, ionic radius, antisymmetric exchange interaction

§1. Introduction

Perovskite-based manganese oxides $RE_{1-X}AE_XMnO_3$ (RE = trivalent rare-earth ions such as La, Pr: AE = divalent alkaline-earth ions such as Sr, Ca) show a variety of dramatic phenomena such as a metal-insulator (MI) transition, a colossal magnetoresistance (CMR) and a field-induced structural transformation.[1,2] By replacing RE^{3+} ions by AE^{2+} ions, Mn^{4+} ions are created and mobile holes are introduced in a low X region, which results in a paramagnetic insulating (PM-I) phase at high temperatures and a ferromagnetic metallic (FM-M) phase at low temperatures. These dramatic properties have been interpreted on the basis of the double-exchange mechanism and the dynamic Jahn-Teller effect etc.[3] For the perovskite-based manganese system, the average radius of A site ions ($RE_{1-X}AE_X$) is also known to play an important role in determining the single particle band-width. For small A site ions which result in a smaller Goldschmidt's tolerance factor ($\Gamma < 1$) the band-width becomes narrow favoring the insulating phase, while for large A site ions ($\Gamma \approx 1$), the metallic properties are enhanced. In the high X region near $X = 1$, mobile electrons are to be doped changing a part of Mn^{4+} ions to Mn^{3+}. In contrast to the hole-doped low X region ($X \leq 0.5$), the investigations for electron-doped high X region are scarce. Several Ca-doped manganese oxides $RE_{1-X}Ca_XMnO_3$ have recently been investigated resulting the existence of a large negative magnetoresistance (MR) effect as in the hole-doped samples. $Bi_{1-X}Ca_XMnO_3$,[4,5] $Eu_{1-X}Ca_XMnO_3$[6] and $Sm_{1-X}Ca_XMnO_3$[7,8] systems all exhibit a canted magnetic order accompanied with the negative MR effect for higher X region ($X > 0.8$). In these Ca-based manganese oxides, there are three common characteristic features; First, the saturation magnetic moment M_s at low temperature shows $1/3 \sim 1/4$ of the fully aligned value. Second, M_s is most enhanced at the Ca concentration of $X \sim 0.90$. Third, the magnetic transition temperature is almost independent of the species of the RE-ions. We denote this ferromagnetic-like order as the canted antiferromagnetic (CAF) order[9] in this paper.

As for $La_{1-X}Ca_XMnO_3$(LCMO) and $Pr_{1-X}Ca_XMnO_3$ (PCMO) systems, both of which are very popular CMR materials, the detailed investigations on the CAF phase and the negative MR effect in the high X region have not been reported. There are several investigations about the magnetic structure in the high X region by means of the powder neutron diffraction technique for these systems. Wollan *et al.* reported that the magnetic structures of the LCMO samples for $X = 0.8$ and $X = 1.0$ are the C-type and G-type antiferromagnetic (AFM) order, respectively.[10] The charge ordering accompanied by the C-type AFM order occurs for $0.5 < X < 0.9$.[9,11] Jirak *et al.* reported on the PCMO system the C-type AFM arrangement below $T_N \sim 170$ K for $X = 0.80$ and G-type alignment below $T_N \sim 110$ K for $X = 1.0$.[12]

In this paper, we study systematically the effect of the radius of the A-site ions on the CAF phase and on the negative MR effect of the lightly electron doped $RE_{1-X}Ca_XMnO_3$ (RE = La, Pr) systems. Especially, we investigate the CAF order and the related negative MR effect of these systems. $La_{0.10}(Ca_{1-y}Sr_y)_{0.90}MnO_3$ ($0 \leq y \leq 0.40$) and $La_{1-X}(Ca_{0.80}Sr_{0.20})_XMnO_3$ ($0.875 \leq X \leq 0.95$) systems are also investigated in order to confirm the correlation between the CAF phase and the average ionic radius of (RE, AE) site. The origin of the CAF phase is also discussed.

§2. Experimental

The $La_{1-X}Ca_XMnO_3$ (LCMO) and $Pr_{1-X}Ca_XMnO_3$ (PCMO) samples ($0.75 \leq X \leq 1.00$) were prepared from stoichiometric mixtures of La_2O_3 (Pr_6O_{11}), $CaCO_3$ and Mn_3O_4 raw powders. The mixtures were calcined at 1000°C for 24 h in air, pressed into pellets and then sintered at 1500°C for 8 h in air. $RE_{0.10}Ca_{0.90}MnO_3$ (RE = Nd, Sm, Gd, Dy), $La_{0.10}(Ca_{1-y}Sr_y)_{0.90}MnO_3$ ($0 \leq y \leq 0.40$) and $La_{1-X}(Ca_{0.80}Sr_{0.20})_XMnO_3$ ($0.875 \leq X \leq 0.95$) samples were also prepared through the same procedures. The samples of the LCMO system were heat-treated at 1500°C for 24 h in flowing O_2 gas to ensure the oxygen stoichiometry. The measured densities of each sample are high, about 80–90% of the ideal one. X-ray diffraction analyses at room temperature confirmed that the samples were in a single phase. The electrical resistivity ρ(T) was measured by a standard four-point probe method under a magnetic field of up to 5 T using a cryocooler cooled superconducting magnet. The magnetization M(T) was measured from 10 to 400 K by a SQUID magnetometer. The thermal dilatation $dL(T)/L$ was measured by a strain gauge method.

§3. Results and Discussion

3.1 $La_{1-X}Ca_XMnO_3$ and $Pr_{1-X}Ca_XMnO_3$

Figures 1(a) and 1(b) show the temperature dependence of the magnetization M(T) for $La_{1-X}Ca_XMnO_3$ and $Pr_{1-X}Ca_XMnO_3$ under an applied field of 0.5 T. With decreasing temperature, M(T) of LCMO in Fig. 1(a) sharply decreases at T_{CO} for $X \leq 0.875$, which suggests the onset of the charge ordering (CO) of Mn^{3+} and Mn^{4+} ions[11] concomitant with the C-type AFM order.[10] For $X \geq 0.90$, M(T) is highly enhanced below T_{CAF} (≈110 K) suggesting the onset of the CAF order, and the depression of M(T) related to CO is wiped out. The spontaneous moment M_s is the largest for $X = 0.90$ and takes about 1/4 of the fully aligned value. For $X = 0.875$, M(T) shows both the depression corresponding to CO and the enhancement corresponding to CAF. LCMO ($X = 0.875$) may not be in a single phase but may consist of a mixture of the CO and CAF phases. For $0.875 \leq X \leq 1.0$, T_{CAF}, which is defined as the onset of M(T) upturn, slightly increases with increasing X; $T_{CAF} \approx 110$ K for $X = 0.875$ and $T_{CAF} \approx 130$ K for $X = 1.0$.

In Fig. 1(b), overall X dependence of M(T) of PCMO is similar to that of LCMO, but there is an important quantitative difference between the two systems; LCMO ($X = 0.875$) shows the M(T) depression correlated to CO, while M(T) of PCMO ($X = 0.875$) shows only M(T) enhancement correlated to the CAF order. The CO transition is noticed only for $X \leq 0.85$ in PCMO. Figure 2 shows the zero field cooled (ZFC) spontaneous moment M_s vs. X of LCMO and PCMO at 10 K under an applied field of 0.5 T. In both systems, M_s is most enhanced at around $X = 0.90$. The M_s value of PCMO ($X = 0.90$) is about 50% larger than that of LCMO ($X = 0.90$). These results imply that the CAF phase is more dominant for PCMO than for LCMO. The main difference between PCMO and LCMO is the difference in the RE ion radius

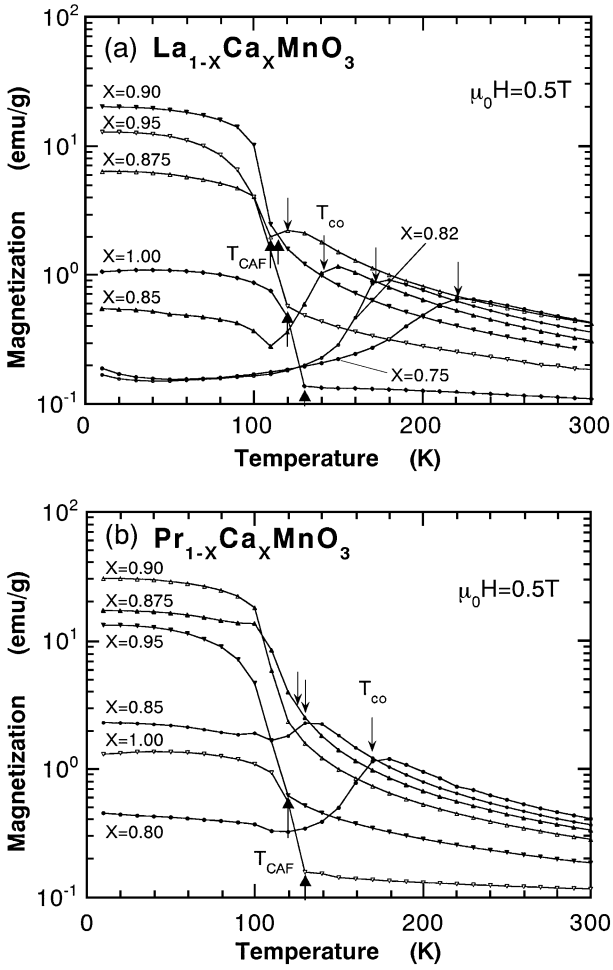

Fig. 1. The temperature dependence of the magnetization M(T) of (a) the $La_{1-X}Ca_XMnO_3$ and (b) the $Pr_{1-X}Ca_XMnO_3$ samples under an applied field of 0.5 T after zero field cooling. The arrows show the charge ordering temperature T_{CO} (↓) and the canted antiferromagnetic ordering temperature T_{CAF} (↑).

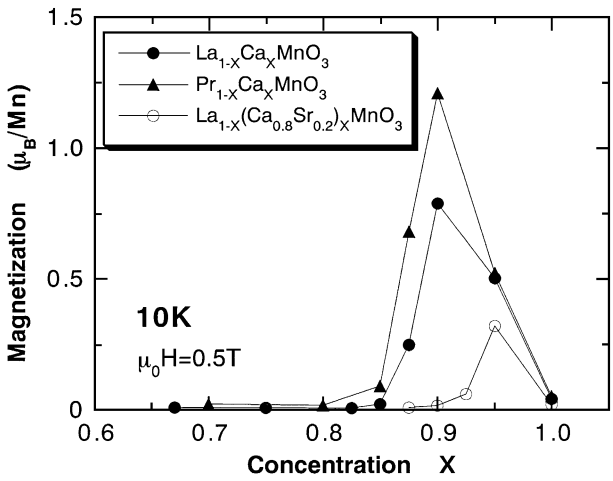

Fig. 2. The spontaneous moment M_s at 10 K as a function of the concentration X for the LCMO and PCMO samples applying 0.5 T after ZFC. M_s vs. X for the $La_{1-X}(Ca_{0.80}Sr_{0.20})_XMnO_3$ is also shown.

r_i (Pr: $r_i = 1.30$ Å, La: $r_i = 1.36$ Å).[13] The M(T) results demonstrate that the smaller r_i of the RE ions favors the CAF phase in the Ca-based manganese systems. The behavior of M(T) as a function of X is analogous to that of

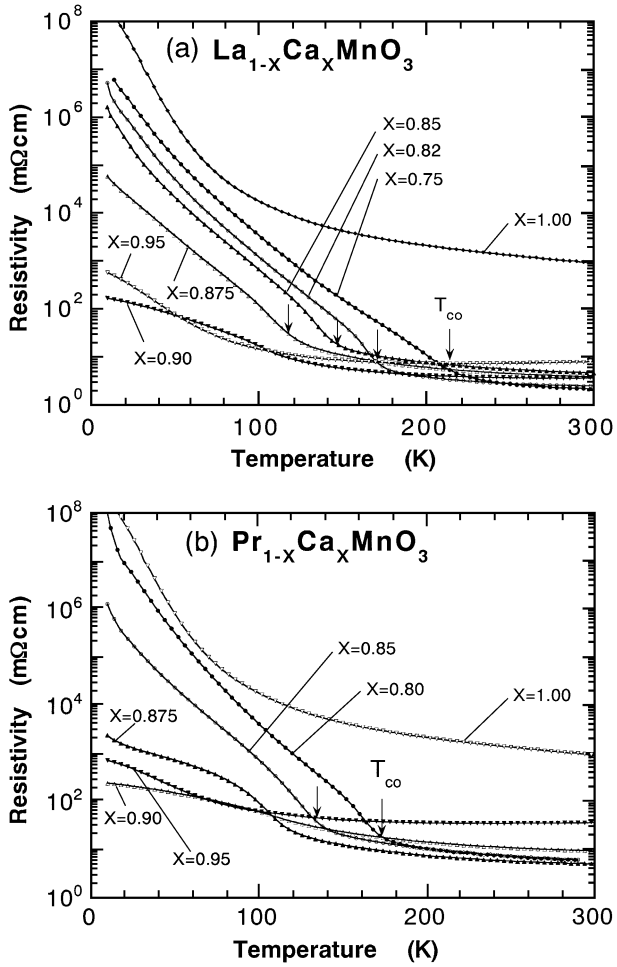

Fig. 3. The temperature dependence of the electrical resistivity ρ(T) of (a) the $La_{1-X}Ca_XMnO_3$ and (b) the $Pr_{1-X}Ca_XMnO_3$ samples. The charge ordering temperature T_{CO} is shown by arrows (↓).

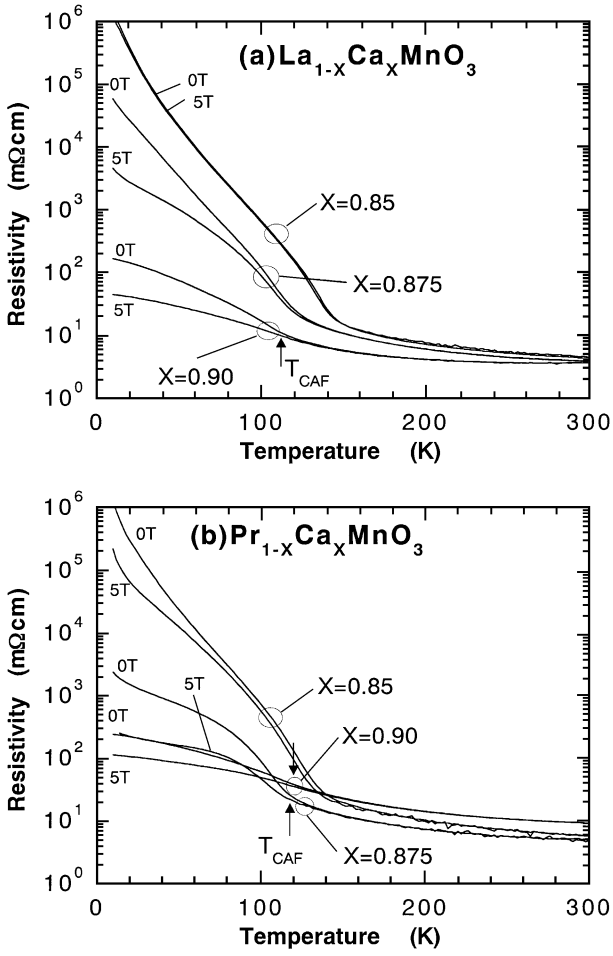

Fig. 4. The temperature dependence of the electrical resistivity ρ(T) of the (a) $La_{1-X}Ca_XMnO_3$ ($X = 0.85$, 0.875 and 0.90) and (b) the $Pr_{1-X}Ca_XMnO_3$ ($X = 0.85$, 0.875 and 0.90) samples under the magnetic field of 5 T. ρ(T) in zero field is also shown for comparison.

$Bi_{1-X}Ca_XMnO_3$[4,5] and $Sm_{1-X}Ca_XMnO_3$[7,8] systems.

Figures 3(a) and 3(b) show the temperature dependence of the electrical resistivity ρ(T) of LCMO and PCMO, respectively. At low temperatures, ρ(T) of all the samples increases with decreasing temperature, showing semiconductive or insulating behavior. Only for $X = 0.95$, both LCMO and PCMO samples slightly show a metallic ρ(T) at high temperatures ($T \geq 200$K). Electron doping into $CaMnO_3$ results in a drastic reduction of ρ(T) in the CAF region and ρ(T) values at low temperatures are the smallest for $X = 0.90$ in both systems. With further electron doping, ρ(T) of the CO phase specimens shows a clear increase below T_{CO}. Comparing $X = 0.875$ samples of LCMO and PCMO, ρ(T) of LCMO is about two orders larger in magnitude than that of PCMO at low temperatures. The ρ value of PCMO ($X = 0.875$) at 10 K is only about an order larger than that of PCMO ($X = 0.90$), while the ρ value of LCMO ($X = 0.875$) is more than two orders larger than of LCMO ($X = 0.90$). These results suggest that, in accord with the M(T) data, the main phase of LCMO ($X = 0.875$) is the CO phase and that the main phase of PCMO ($X = 0.875$) is the CAF phase.

Figures 4(a) and 4(b) show ρ(T) of the typical LCMO and PCMO samples in an applied magnetic field of 5 T. ρ(T) in zero field is also shown for comparison. Large negative MR is observed for the CAF phase samples below T_{CAF}, making a marked contrast to the CO phase samples which show almost no MR. Figure 5 presents the electrical conductivity enhancement (positive magnetoconductance) at 10 K caused by the applied field, i.e., $\Delta\sigma = \sigma(5\,\mathrm{T}) - \sigma(0\,\mathrm{T})$, for LCMO and PCMO. The conductivity measurements were performed under a field-cooled (FC) condition. $\Delta\sigma$ is the largest for $X = 0.90$ in both systems. $\Delta\sigma$ of LCMO is larger than that of PCMO for $X = 0.90$. Since Pr has a smaller ion radius than Ca, the Pr substitution reduces the tolerance factor Γ and enhances the lattice distortion of the perovskite structure. The lattice distortion from cubic is known to reduce the single electron bandwidth ΔW. Then the electrons in LCMO are expected to be more easy to transfer than in PCMO. The enhanced magnetoconductivity $\Delta\sigma$ in LCMO may be related to the difference of the ΔW values between LCMO and PCMO. For $X = 0.875$, $\Delta\sigma$ of LCMO is very small, while $\Delta\sigma$ of PCMO ($X = 0.875$) is nearly as large as that of PCMO ($X = 0.90$). These results clearly demonstrate again that the main phase of PCMO ($X = 0.875$) is the CAF phase and that of LCMO ($X = 0.875$) is the CO phase.

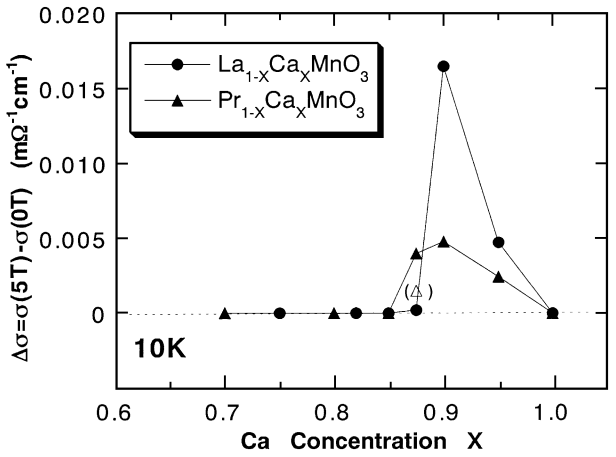

Fig. 5. The electrical conductivity enhancement at 10 K, $\Delta\sigma(\mathrm{H}) = \sigma(5\,\mathrm{T}) - \sigma(0\,\mathrm{T})$, caused by the applied field of 5 T after the field cooling for the LCMO and PCMO samples. An open triangle represents the $\Delta\sigma$(H) on the zero field cooling condition for the $La_{0.125}Ca_{0.875}MnO_3$ sample (see text).

3.2 On a possible field induced lattice transformation in $Pr_{0.125}Ca_{0.875}MnO_3$

For the PCMO ($X = 0.875$) sample, we have found a significant difference between FC and ZFC ρ(T) and M(T) data as Figs. 6(a) and 6(b) demonstrate. The difference between the FC and ZFC data is very small for $X = 0.90$. In contrast, we see a large difference between FC and ZFC results for $X = 0.875$. On the ZFC condition, the positive magnetoconductivity $\Delta\sigma$ is reduced to about 2/5 of the FC data as shown by a open triangle in Fig. 5. In Fig. 6(b), the M(T) value of ZFC PCMO ($X = 0.875$) is reduced to about 2/3 of FC PCMO ($X = 0.875$) at 10 K. Figures 7(a) and 7(b) show the field dependence of $\Delta\sigma$(H) and M(H) at 10 K for ZFC PCMO ($X = 0.875$). In Fig. 7(a), $\Delta\sigma$(H) ($= \sigma(\mathrm{H}) - \sigma(0\,\mathrm{T})$) shows a pretty large hysteresis effect between up and down field scans; after the field scan up to 5 T, the conductivity in zero-field increases by about 10%. The M(H) curve in Fig. 7(b) also shows a hysteresis behavior, though it is very small in comparison to the corresponding hysteresis of $\Delta\sigma$(H).

Now let us discuss a possible origin of the observed hysteresis behavior of PCMO ($X = 0.875$). Figure 8 presents the thermal dilatation $\mathrm{d}L/L$ vs. T of PCMO ($0.80 \leq X \leq 1.0$). With decreasing T, $\mathrm{d}L/L$ shows an anomalous shrink at T_{CAF} for $X \geq 0.875$ and at T_{CO} for $X \geq 0.850$. The contraction of the sample at T_{CAF} and T_{CO} suggests that a kind of structural transformation may take place accompanied with these phase transitions of PCMO. Jirak *et al.*[12] observed by the low temperature neutron diffraction an elongated pseudotetragonal (T′) structure for $0.75 \leq X \leq 0.90$ and pseudocubic (C) structure for $0.90 \leq X \leq 1.0$. These results suggest that the lattice structure of PCMO in the CAF phase ($0.875 \leq X \leq 1.0$) is pseudocubic and that of PCMO in the CO phase ($0.80 \leq X \leq 0.85$) is pseudotetragonal. Jirak *et al.* also observed a two-phase structure for PCMO ($X = 0.90$). It is possible that the present PCMO ($X = 0.875$) sample has the two-phase structure because its Pr concentration is near the boundary (X_{C})

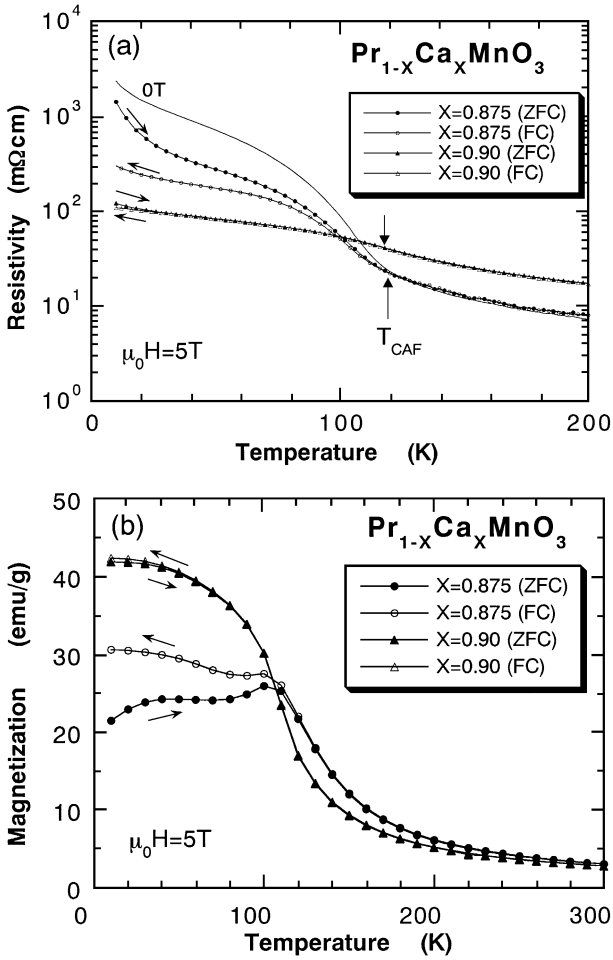

Fig. 6. (a) The temperature dependence of the electrical resistivity ρ(T) of $Pr_{1-X}Ca_XMnO_3$ ($X = 0.875$ and 0.90) samples under an magnetic field of 5 T (ZFC and FC scans). (b) The magnetization M(T) of the same samples as a function of T under an magnetic field of 5 T (ZFC and FC scans).

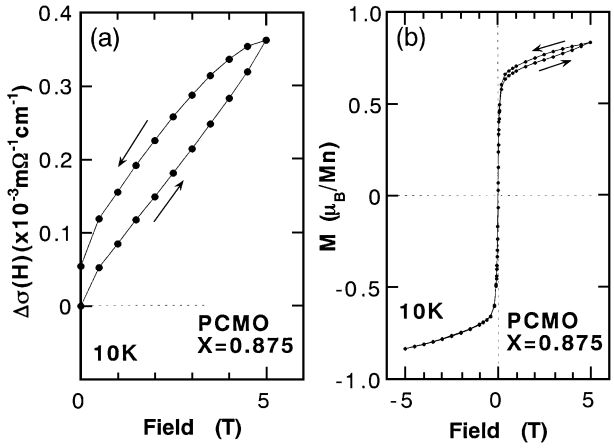

Fig. 7. (a) The electrical conductivity enhancement at 10 K, $\Delta\sigma(H) = \sigma(\mathrm{H}) - \sigma(0\,\mathrm{T})$ caused by the applied field after the zero field cooling for the PCMO ($X = 0.875$) sample. (b) Magnetization curve at 10 K for the same sample.

between the CAF and CO phases. On FC condition in a field of 5 T, a larger part of the PCMO ($X = 0.875$) may transform to the pseudocubic structure with the spontaneous moment M_{s} and M_{s}(T) in Fig. 6(b) is enhanced in this case. Since only the CAF phase exhibits the large

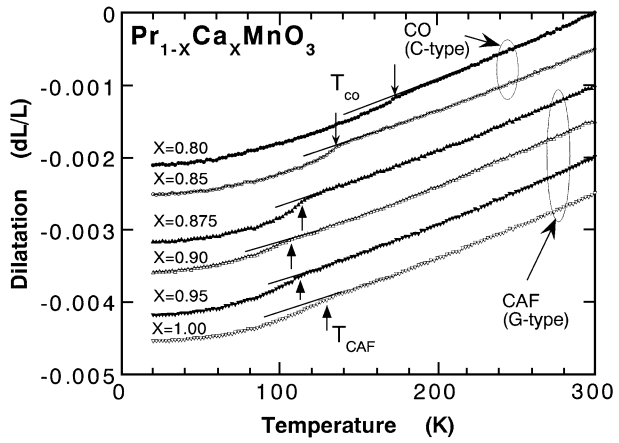

Fig. 8. Temperature dependence of the thermal dilatation dL(T)/L for the $Pr_{1-X}Ca_XMnO_3$ samples. Downward arrows (↓) indicate the charge ordering temperature T_{CO} and upward arrows (↑) indicate the canted antiferromagnetic temperature T_{CAF}.

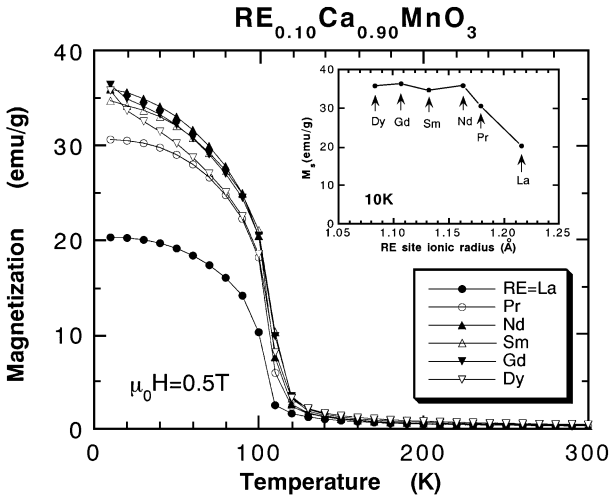

Fig. 9. The temperature dependence of the magnetization M(T) of $RE_{0.10}Ca_{0.90}MnO_3$ samples (RE = La, Pr, Nd, Sm, Gd, Dy). The inset shows the saturation moment M_s at 10 K as a function of the ionic radius of RE ions.

negative MR effect, the FC ρ(T) of PCMO ($X = 0.875$) in Fig. 6(a) shows larger negative MR effect in comparison to ZFC ρ(T).The hysteresis behaviors of $\Delta\sigma$(H) in Fig. 7(a) and M(H) in Fig. 7(b) suggest that a small part of PCMO ($X = 0.875$) makes the lattice transformation even at 10 K in an applied field of 5 T. The characteristic hysteresis behavior of ρ and M_s between FC and ZFC conditions was not observed LCMO ($X = 0.875$) probably because the CO phase is overwhelmingly dominant over the CAF phase in this sample.

3.3 $RE_{0.10}Ca_{0.90}MnO_3$ (RE=Pr, Nd, Sm, Dy)

The CAF phase and the related large negative MR effect are peculiar and common characters for the electron-doped Ca-base manganese ($X \sim 0.9$) and the smaller ionic radius of RE ions seems to enforce the CAF state. In order to confirm the effect of the ionic radius of RE ions on the CAF phase, the magnetization M(T) of $RE_{0.10}Ca_{0.90}MnO_3$ samples (RE = Nd, Sm, Gd, Dy) with a fixed concentration $X = 0.90$ was measured. Figure 9 shows the M(T) curves of these samples under the magnetic field of 0.5 T together with those of the LCMO and PCMO. The inset shows M_s as a function of r_i of RE ions.[13] Although the CAF phase was confirmed below nearly the same temperature T_{CAF} (∼110 K) irrespective of the ionic radius of RE ions, the saturation moment M_s increases with decreasing ionic radius of RE ions for La, Pr, Nd, showing no dependence for smaller RE ions (Nd, Sm, Gd, Dy). The negative MR effect similar to the LCMO and PCMO systems was also observed for these materials.

3.4 $La_{0.10}(Ca_{1-y}Sr_y)_{0.90}MnO_3$ and $La_{1-X}(Ca_{0.80}Sr_{0.20})_XMnO_3$

Our experimental results on electron doped $RE_{1-X}Ca_XMn\ O_3$ have clearly indicated the importance of A site ion radius for the CAF phase stabilization. A more direct way to change the A site ion radius is to substitute Ca by Sr with a larger ionic radius. Figures 10(a) and 10(b) show M(T) and ρ(T) of

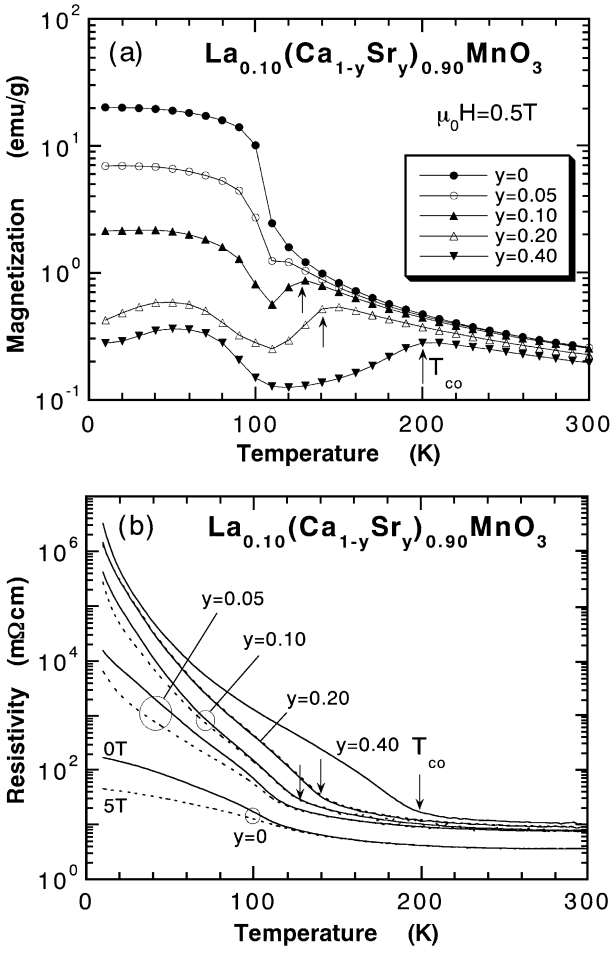

Fig. 10. (a) The magnetization M(T) and (b) the electrical resistivity ρ(T) of the $La_{0.10}(Ca_{1-y}Sr_y)_{0.90}MnO_3$ ($0 \le y \le 0.4$) system with a fixed AE ion concentration $X = 0.90$. Arrows indicate the charge ordering temperature T_{CO}.

$La_{0.10}(Ca_{1-y}Sr_y)_{0.90}MnO_3$ ($0 \le y \le 0.40$). By substituting only 5% Ca by Sr, the saturation moment M_s drastically decreases and for $y = 0.10$, M_s reduces to just 1/10 of $La_{0.10}Ca_{0.90}MnO_3$. With increasing y, the

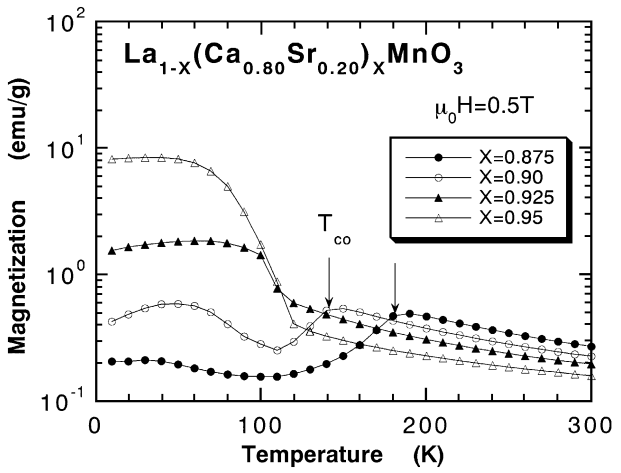

Fig. 11. The magnetization M(T) of the $La_{1-X}(Ca_{0.80}Sr_{0.20})_X MnO_3$ system ($0.875 \leq X \leq 0.95$) with a fixed Sr ion content $y = 0.20$. Arrows indicate the charge ordering temperature T_{CO}.

depression of M(T) which corresponds to the CO onset appears and for $y = 0.10$, the CO transition can be clearly confirmed in Fig. 10(a). In Fig. 10(b), ρ(T) drastically increases with increasing y. The negative MR effect can be seen up to $y = 0.10$, but the positive magnetoconductivity $\Delta\sigma$(H) is very small for $y = 0.10$. The $y = 0.10$ sample may not be in a single phase and its main phase may be the CO phase. The properties of $La_{0.10}(Ca_{0.90}Sr_{0.10})_{0.90}MnO_3$ are very similar to those of $La_{0.125}Ca_{0.875}MnO_3$.

Figure 11 shows M(T) of the $La_{1-X}(Ca_{0.80}Sr_{0.20})_X MnO_3$ samples. In this $(Ca_{0.80}Sr_{0.20})$-based system with large RE and AE ionic radius, the CAF phase is very rapidly quenched with decreasing X. For $X = 0.95$, M(T) of this system shows a pretty large M_s at low temperatures characteristic of the CAF phase. But M_s is remarkably reduced for the $X = 0.925$ sample and the CAF is already greatly damaged at this concentration. As can be seen in this figure, a distinct depression of M(T) with decreasing T characteristic of the CO phase is noticeable for $X = 0.90$ and $La_{0.10}(Ca_{0.80}Sr_{0.20})_{0.90}MnO_3$ clearly belongs to the CO phase. Thus in this system, the CAF phase is dominant in a very narrow region of $X \geq 0.925$. This fact makes a marked contrast to Ca-based compounds because all the $RE_{0.10}Ca_{0.90}MnO_3$ studied in this paper shows the largest M_s for $X = 0.90$. M_s vs. X of $La_{1-X}(Ca_{0.80}Sr_{0.20})_X MnO_3$ is also contained in Fig. 2.

3.5 The CAF state vs. the CO state in $RE_{1-X}AE_X MnO_3$ in the electron doping region

As we have seen in the preceding subsections, the larger A-site ion radius results in a drastic deterioration of the CAF phase. Thus the experimental results for both RE ion substituted and AE ion substituted $RE_{1-X}AE_X MnO_3$ systems indicate the important role of the A site ionic radius. Figure 12 shows the phase diagram of the CO and CAF phases as a function of the AE ion concentration X and the average ionic radius of A site. In this figure, open circles represent the occurence of the CO phase and the closed circles represent the realization of the CAF phase.

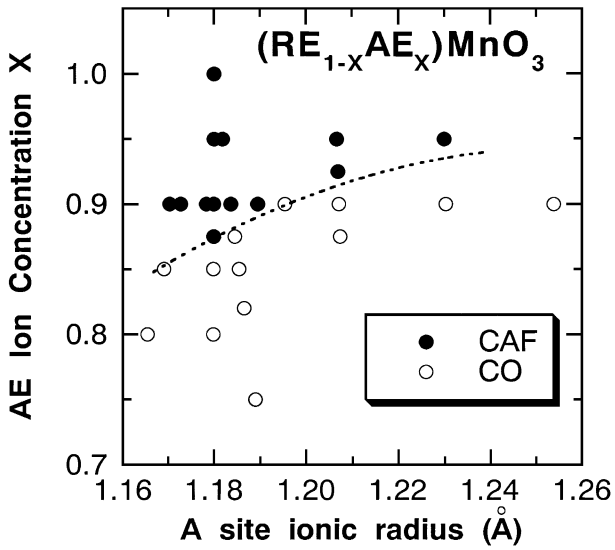

Fig. 12. The phase diagram of the relation between the CO and the CAF phases as a function of the AE ion concentration X and the average ionic radius of (RE,AE) site in the $RE_{1-X}AE_X MnO_3$ system. Open circles represent the CO phase and closed circles represent the CAF phase. The ionic radius was calculated from the tabulated radii with ninth-fold coodination.[13)]

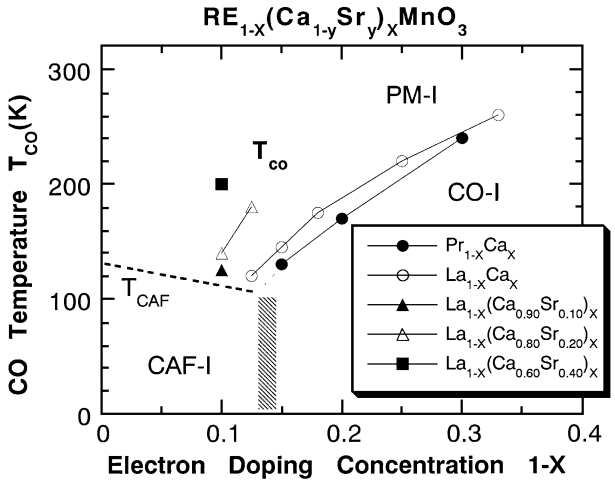

Fig. 13. The CO transition temperature T_{CO} determined in this work as a function of the electron doping concentration $1 - X$.

The critical concentration X_C which separates the two phases increases with increasing average radius of A-site ions. Figure 13 represents the CO transition temperature T_{CO} studied in this work as a function of the electron doping concentration $1 - X$. The average A site ionic radius becomes smaller in the consecutive order of $La_{0.10}(Ca_{0.60}Sr_{0.40})_{0.90}$, $La_{0.10}(Ca_{0.80}Sr_{0.20})_{0.90}$ and $La_{0.10}(Ca_{0.90}Sr_{0.10})_{0.90}$, $La_{0.10}Ca_{0.90}$ and $Pr_{0.10}Ca_{0.90}$. Figure 13 clearly demonstrates that the larger A site ionic radius always results in a higher T_{CO} at a fixed value of electron-doping $1 - X$. It is worthwhile to note that the larger A site ionic radius, which should result in a larger tolerance factor Γ and a wider single particle band-width, seems to favor the CO phase in this electron-doping region.

3.6 On the origin of the CAF state

The crystal structure of $CaMnO_3$ is actually orthorhombic at low temperatures with space group *pbmn*,[14] which has no inversion symmetry at the midpoint of the nearest Mn^{4+} spins. In this lattice, Dzyaloshinsky-Moriya (DM) antisymmetric exchange interaction[15] is possible. The DM interaction results in the weak ferromagnetism (WF) with a canted spin configuration in an antiferromagnet. The antiferromagnetic structure in the region of X where the CAF phase occurs were reported to be the G-type. The G-type structure is suitable for WF because all the nearest neighbor Mn spins are oriented antiparallel; parallel spin pairs cannot contribute to WF. In contrast, in the region of X where the CO phase dominates, the reported C-type structure consists of ferromagnetic chains mutually oriented antiparallel.

As is shown in Fig. 2, the WF spontaneous moment M_s is drastically enhanced by a small amount Ca substitution by La or Pr while the magnetic ordering temperature T_{CAF} remains almost constant. The nearly constant T_{CAF} suggests that the antiferromagnetic superexchange which mainly determines T_{CAF} is not so much affected by initial Ca substitution. The drastic M_s enhancement suggests the drastic enhancement of the DM interaction. Qualitatively, the reduction in the local symmetry between Mn spins is expected to enhance the DM interaction. The Ca substitution by RE ions reduces the local symmetry between near Mn spins and the symmetry reduction effect should be stronger for the smaller RE ion because of the stronger mismatch of the ionic radius against Ca ions. It is very probable that the DM interaction is more strongly enhanced by the smaller RE ion substitution and the DM interaction seems to be a key factor for the canted AF state in electron-doped $RE_{1-X}Ca_XMnO_3$.

In contrast to the hole-doped ferromagnetic region,[16] where the double exchange mechanism is dominant, the canted antiferromagnetic transition does not accompany any reduction of ρ(T) at or below T_{CAF}. However, the double exchange-like mechanism,[17,18] through which the doped electrons hop between parallel Mn^{4+} spin sites enhancing the ferromagnetic component, may simultaneously be at work because the absolute values of ρ(T) are significantly reduced as a whole and the negative MR effect is conspicuous in the CAF phase. The DM antisymmetric exchange interaction and the double exchange mechanism may cooperatively stabilize the CAF phase in the $RE_{1-X}AE_XMnO_3$ systems near $X = 1.0$.

§4. Summary

The magnetization M(T) and the electrical resistivity ρ(T) of lightly electron-doped $La_{1-X}Ca_XMnO_3$, $Pr_{1-X}Ca_XMnO_3$ and other $RE_{1-X}AE_XMnO_3$ (RE; rare-earth, AE; alkaline-earth) have been measured. Important experimental results and the noticeable points obtained in this study are summarized as follows;

(1) The canted antiferromagnetic (CAF) phase and the related large negative magnetoresistance were observed for $RE_{1-X}Ca_XMnO_3$ (RE = La, Pr, Nd, Sm, Gd, Dy) for $X > 0.90$ and the charge ordered (CO) phase was found for $X < 0.90$. The boundary concentration X_C between the CAF and CO phase depends on the RE ion radius. The CAF phase became dominant over the CO phase for smaller RE ion radius. The spontaneous magnetic moment M_s in the CAF phase also increased for the smaller RE ions.

(2) The substitution of Ca by Sr in the $La_{0.10}(Ca_{1-y}Sr_y)_{0.90}$ MnO_3 system promptly depressed the CAF order, enforcing the CO phase. The result implies that the CAF phase become dominant also for the smaller average AE ion radius.

(3) The phase boundary between the CAF and the CO phase was determined as a function of the AE concentration X and the A site ion radius.

(4) Distinct differences were observed for field-cooled and zero-field-cooled ρ(T) and M(T) of $Pr_{0.125}Ca_{0.875}MnO_3$. A possibility of field-induced structural transformation was suggested in this PCMO ($X \approx X_C$) sample.

(5) As a origin of the CAF phase, the importance of Dzyaloshinsky-Morita antisymmetric exchange interaction was pointed out.

Acknowledgment

The authors wish to thank Prof. T. Fukase of the Institute for Materials Research, Tohoku University, for valuable discussions. The authors also wish to thank T. Kikuchi and T. Fujiwara of Iwate University for their assistance in the sample preparation. This work is partially supported by the REIMEI Research Resources of Japan Atomic Energy Research Institute.

1) H. Yoshizawa, H. Kawano, Y. Tomioka and Y. Tokura: J. Phys. Soc. Jpn. **65** (1996) 1043.
2) Y. Tomioka, A. Asamitsu, Y. Morimoto, H. Kuwahara and Y. Tokura: Phys. Rev. Lett. **74** (1995) 5108.
3) A. J. Millis, P. B. Littlewood and B. I. Shaiman: Phys. Rev. Lett. **74** (1995) 5144.
4) H. Chiba, M. Kikuchi, K. Kusaba, Y. Muraoka and Y. Shono: Solid State Commun. **99** (1996) 499.
5) Wei Bao, J. D. Axe, C. H. Chen and S.-W. Cheong: Phys. Rev. Lett. **78** (1997) 543.
6) I. O. Troyanchuk, N. V. Samsonnenko, H. Szymczak and A. Nabialek: J. Solid State Chem. **131** (1997) 144.
7) C. Martin, A. Maignan, F. Damay and B. Raveau: J. Solid State Chem. **134** (1997) 198.
8) A. Maignan, C. Martin, F. Damay, B. Reveau and J. Hejtmanek: Phys. Rev. B **58** (1998) 2758.
9) A. J. Millis: Nature **392** (1998) 147.
10) E. O. Wollan and W. C. Koehler: Phys. Rev. **100** (1955) 545.
11) A. P. Ramirez, P. Schiffer, S.-W. Cheong, C. H. Chen, W. Bao, T. T. M. Palstra, P. L. Gammel, D. J. Bishop and B. Zegarski: Phys. Rev. Lett. **76** (1996) 3188.
12) Z. Jirak, S. Krupicka, Z. Simsa, M. Dlouha and S. Vratislav: J. Mag. Mag. Mater. **53** (1985) 153.
13) R. D. Shannon: Acta. Crystallegr. A **32** (1976) 751.
14) K. R. Poeppelmeiner, M. E. Leonowicz, J. C. Scanlon, J. M. Longo and W. B. Yelon: J. Solid State. Chem. **43** (1982) 1137.
15) E. A. Turov: *Physical Properties of Magnetically Ordered Crystals*, (Academic Press, New York and London 1965).
16) H. Fujishiro, T. Fukase, M. Ikebe and T. Kikuchi: J. Phys. Soc. Jpn. **68** (1999) 1469.
17) C. Zener: Phys. Rev. **82** (1951) 403.
18) P. G. de Gennes: Phys. Rev. **118** (1960) 141.